

In silico design of a new Zn–triazole based metal–organic framework for CO₂ and H₂O adsorption

Cite as: J. Chem. Phys. **154**, 024303 (2021); <https://doi.org/10.1063/5.0037594>

Submitted: 16 November 2020 . Accepted: 22 December 2020 . Published Online: 12 January 2021

 R. Dahmani,  S. Grubišić,  I. Djordjević, S. Ben Yaghlane, S. Boughdiri,  G. Chambaud, and  M. Hochlaf

COLLECTIONS

Paper published as part of the special topic on [Special Collection in Honor of Women in Chemical Physics and Physical Chemistry](#)



View Online



Export Citation



CrossMark

ARTICLES YOU MAY BE INTERESTED IN

[Model DFT exchange holes and the exact exchange hole: Similarities and differences](#)

The Journal of Chemical Physics **154**, 024101 (2021); <https://doi.org/10.1063/5.0031995>

[Characterization of a vacuum ultraviolet light source at 118 nm](#)

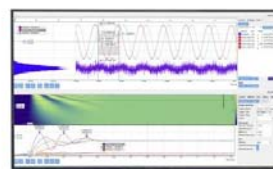
The Journal of Chemical Physics **154**, 024201 (2021); <https://doi.org/10.1063/5.0033135>

[Tuning the hexane isomer separation performances of Zeolitic Imidazole Framework-8 using mechanical pressure](#)

The Journal of Chemical Physics **154**, 084702 (2021); <https://doi.org/10.1063/5.0040469>

Challenge us.

What are your needs for
periodic signal detection?



Zurich
Instruments

In silico design of a new Zn-triazole based metal-organic framework for CO₂ and H₂O adsorption

Cite as: J. Chem. Phys. 154, 024303 (2021); doi: 10.1063/5.0037594

Submitted: 16 November 2020 • Accepted: 22 December 2020 •

Published Online: 12 January 2021



R. Dahmani,^{1,2} S. Grubišić,^{3,a)} I. Djordjević,³ S. Ben Yaghlane,⁴ S. Boughdiri,² G. Chambaud,^{1,a)} and M. Hochlaf^{1,a)}

AFFILIATIONS

¹ Université Gustave Eiffel, COSYS/LISIS, 5 Bd Descartes, 77454 Champs sur Marne, France

² Université de Tunis El Manar, Faculté des Sciences de Tunis, Laboratoire de Caractérisations, Applications et Modélisation des Matériaux – LR18ES08, Tunis, Tunisia

³ University of Belgrade – Institute of Chemistry, Technology and Metallurgy, Department of Chemistry, Njegoševa 12, 11000 Belgrade, Republic of Serbia

⁴ Université de Tunis El Manar, Faculté des Sciences de Tunis, Laboratoire de Spectroscopie Atomique, Moléculaire et Applications – LSAMA, 2092 Tunis, Tunisia

Note: This paper is part of the JCP Special Collection in Honor of Women in Chemical Physics and Physical Chemistry.

^{a)} **Authors to whom correspondence should be addressed:** grubisic@chem.bg.ac.rs; gilberte.chambaud@univ-eiffel.fr; and hochlaf@univ-mlv.fr

ABSTRACT

In search for future good adsorbents for CO₂ capture, a nitrogen-rich triazole-type Metal-Organic Framework (MOF) is proposed based on the rational design and theoretical molecular simulations. The structure of the proposed MOF, named Zinc Triazolate based Framework (ZTF), is obtained by replacing the amine-organic linker of MAF-66 by a triazole, and its structural parameters are deduced. We used grand-canonical Monte Carlo (GCMC) simulations based on generic classical force fields to correctly predict the adsorption isotherms of CO₂ and H₂O. For water adsorption in MAF-66 and ZTF, simulations revealed that the strong hydrogen bonding interactions of water with the N atoms of triazole rings of the frameworks are the main driving forces for the high adsorption uptake of water. We also show that the proposed ZTF porous material exhibits exceptional high CO₂ uptake capacity at low pressure, better than MAF-66. Moreover, the nature of the interactions between CO₂ and the MAF-66 and ZTF surface cavities was examined at the microscopic level. Computations show that the interactions occur at two different sites, consisting of Lewis acid-Lewis base interactions and hydrogen bonding, together with obvious electrostatic interactions. In addition, we investigated the influence of the presence of H₂O molecules on the CO₂ adsorption on the ZTF MOF. GCMC simulations reveal that the addition of H₂O molecules leads to an enhancement of the CO₂ adsorption at very low pressures but a reduction of this CO₂ adsorption at higher pressures.

Published under license by AIP Publishing. <https://doi.org/10.1063/5.0037594>

I. INTRODUCTION

The increasing amounts of greenhouse gases cause changes in terrestrial ecosystems and contribute to the global climate change.¹ In that context, the prevention of the climate change is a huge universal challenge. Different approaches have been developed to reduce CO₂ emissions, among which adsorption of gases on solid

materials is already well known and used in industries for gas separation and purification because of its low energy consumption compared to other separation processes such as chemical absorption.²

The advances in using metal organic frameworks (MOFs) as adsorbent materials for CO₂ capture have been extensively investigated³ owing to their favorable properties such as their large

surface area, permanent porosity, and tunable pore size/functionality. These adsorbent materials can be synthesized by adding an organic ligand and a metallic salt to form a three-dimensional crystalline structure with well-defined pore sizes. The MOFs interact with adsorbate through several types of interactions including van der Waals type interactions, metal-substrate interactions, and hydrogen bonds.⁴ The investigation of adsorption phenomena at the microscopic level can be realized through molecular simulation techniques such as Grand Canonical Monte Carlo (GCMC) coupled to density functional theory (DFT) approaches. Indeed, such approaches have been widely used to understand the mechanism of CO₂ adsorption isotherms in porous materials.

Lin *et al.*⁵ demonstrated experimentally the exceptional CO₂ adsorption capacity through the newly synthesized triazolate framework, 3-amino-1,2,4-triazolate (Atz⁻), named MAF-66 with uncoordinated triazolate N donors exposed on the pore surface and the amino group at position 3 of 1,2,4-triazolate. Thus, the addition of an uncoordinated nitrogen atom creates a new adsorption site for CO₂ through the Lewis acid–base interaction between the basic nitrogen and the acidic carbon of CO₂. It is worth noting also that amino groups may participate indirectly in the adsorption of CO₂ in MOFs. Indeed, Stavitski *et al.*⁶ showed that the adsorption of CO₂ on the NH₂-MIL-53 (Al) framework is directed by the formation of rather weak hydrogen bonds between CO₂ and bridging hydroxyl groups of the lattice of the investigated MOF. However, other groups showed that when the amino groups are attached to the organic linker of the MOFs and do not directly interact with CO₂, no enhancement of CO₂ capture is observed. This was reported by Serra-Crespo *et al.*,⁷ who showed that van der Waals interactions between the adsorbate and the adsorbent are responsible for the adsorption process between NH₂-MIL-101(Al) and CO₂, without any direct chemical interaction between amino groups and CO₂.

Open metal MOFs are among the most promising CO₂ capture materials due to the favorability of their coordinatively unsaturated metals as binding sites for adsorbates. They are viewed as attractive materials for CO₂ as well as H₂O adsorption. In natural and industrial media, both CO₂ and H₂O molecules are commonly present together, and competition between them within the MOFs pores may take place. This may induce an enhancement or a decrease in the CO₂ capture. Some effects, either positive or negative, on the selectivity of these materials toward CO₂ are also expected. The sequestration of CO₂ could be modified in the presence of water molecules, where the surface of the MOF pores may react with water, enhancing or decreasing thus locally their Brønsted acidity.^{8–13} These benefits or drawbacks are still not well understood at the microscopic level, which is mandatory for controlling the macroscopic properties related to the CO₂ adsorption in nanoporous materials and for the purification of clean-burning natural gas.

In a recent review, Burtch *et al.*¹⁴ pointed out that water stability of adsorbents, such as nanoporous materials, is affected by steric effects in the vicinity of the ligand and by the nature of the coordination sites in these materials. On the other hand, recent investigations on zeolitic imidazolate frameworks (ZIFs), and related compounds, showed that the increase in the number of nitrogen atoms within the heterocycle of the organic linker is favorable for CO₂ adsorption and an increase of the CO₂ uptake is observed.^{15–18} Among them,

triazoles exhibit exceptional capacity and selectivity for gas adsorption. This is related to the strong interactions between CO₂ and amine functionalities as pointed out above.^{19–22} Therefore, the combination of tetrahedral metallic ions such as Zn(II) and triazole ligands, giving isomeric triazolate based MOFs with zeolite-like topologies, seems to be a good proposal to increase the capture of CO₂ compared to imidazole based ZIFs due to the presence of one more nitrogen in triazoles' aromatic ring than in imidazole one.

Recently, we investigated the stable structures of the non-reactive and reactive clusters formed between Zn²⁺-triazoles ([Zn²⁺-Tz]) and CO₂ and/or H₂O, where [Zn²⁺-Tz] are the subunits of triazolate based MOFs.²³ Several binding sites are found between these subunits and CO₂/H₂O, where the organometallic complex interacts with CO₂/H₂O either by covalent or weak interactions (hydrogen bonds, van der Waals type). Upon complexation, intramolecular proton transfers are also observed. Moreover, this work showed that water induces huge changes on the energy profiles of tautomeric reactions converting one [Zn²⁺-Tz] isomer to another. In sum, we have found a multitude of physical and chemical phenomena that are occurring at the microscopic level when H₂O is close to the [Zn²⁺-Tz] subunits. We suggested thus the consideration of traces of water in the pores to better model the behavior of CO₂ (sequestration and reactivity) on nanoporous materials used in industrial applications. To this end, we present here the investigations of CO₂/H₂O interacting with MAF-66 as well as with a model MOF based on [Zn²⁺-2A]_a and [Zn²⁺-2A]_b isomers of [Zn²⁺-Tz] that we identified in our recent work.²⁴

We used the DFT method to optimize the structures of MAF-66 and of our proposed MOF porous material. Initial models of MOFs were constructed starting from the crystal structure of MAF-66.⁵ The proposed MOF, labeled hereafter ZTF (for zinc triazolate based framework), was built by replacing the NH₂ group of the triazolate ring of MAF-66 by an hydrogen atom in order to get a more accessible pore surface for CO₂ capture. These materials are highly porous metal triazolate frameworks, functionalized with high density uncoordinated N donors on the pore size.²⁵ The adsorption of H₂O in MAF-66 and ZTF was also explored by force-field based Monte Carlo simulations in order to unravel the atomistic mechanisms that control water uptakes in this hydrolytically stable porous material. In addition, we performed grand-canonical Monte Carlo (GCMC) simulations based on generic classical force fields to compute the adsorption isotherms of CO₂, with and without the presence of H₂O molecules inside MAF-66 and ZTF MOFs. Besides, H₂O and CO₂ were introduced in competition where the number of preloaded H₂O molecules in ZTF was increased from 0 to 100 and allowed to move until reaching equilibrium. In the presence of water molecules, we considered two levels of hydration: (i) water molecules were introduced at the active sites in ZTF such as uncoordinated nitrogen N of triazolate ring where they are located in the vicinity of nitrogen through N–H(OH) interaction with $d_{N \dots H} \sim [1.78–1.81] \text{ \AA}$; (ii) around coordinatively “unsaturated” Zn atoms in which H₂O interacts through the oxygen atom and zinc, with $d_{Zn \dots O} \sim [2.17 \text{ \AA}–2.44 \text{ \AA}]$. In order to include coordinated water in our simulations, we considered hydration in which one or two H₂O molecules are present per metal corner. Computations show that the effect of water on the CO₂ adsorption depends on the pressure and on the number of preloaded water molecules into the cavity. Throughout this manuscript, we followed the commonly admitted

terminology for the coordination of the metal center [Zn(II)] as “unsaturated,” rather than “complete,” despite that this metal is coordinated to four triazoles. Indeed, these sites within the MOFs remain accessible to guest molecules such as CO₂ or H₂O where the electronic deficiency of metal sites produces strong interactions with electronic donors (guest molecules).

II. COMPUTATIONAL DETAILS

Periodic DFT calculations have been performed with the SIESTA^{26,27} suite of programs by using the generalized gradient approximation (GGA) Perdew, Burke, and Ernzerhof (PBE) functional.²⁸ These computations consist of optimizing the structure of MAF-66 and ZTF, as well as the positions of H₂O and CO₂ molecules inside the pores. We used double zeta polarized (DZP) basis sets and norm conserving pseudo potentials for all calculations. Based on convergence tests (Fig. S1), real space integrals were performed on a mesh with a 200 Ry cutoff. Geometry optimizations were done in such a way to allow full atomic and cell relaxation without geometrical constraints up to a force threshold of 0.05 eV/Å. The Brillouin zone was sampled by the 4 × 4 × 4 Γ -centered Monkhorst–Pack k-point.

Adsorption energies, ΔE_{ads} , for CO₂ and H₂O molecules are calculated using the following equations:

$$\Delta E_{\text{ads}}(\text{CO}_2) = E_{Zc} - (E_{\text{MOF}} + E_{\text{CO}_2}), \quad (1)$$

$$\Delta E_{\text{ads}}(\text{H}_2\text{O}) = E_{Zh} - (E_{\text{MOF}} + E_{\text{H}_2\text{O}}), \quad (2)$$

where E_{Zc} and E_{Zh} represent the total energies of MOFs (ZTF and MAF-66) containing a CO₂ or H₂O molecule; E_{MOF} is the total energy of the same MOF without adsorption of carbon dioxide and water. E_{CO_2} and $E_{\text{H}_2\text{O}}$ are the total energies of the isolated molecules evaluated using a supercell with a dimension of $10 \times 10 \times 10 \text{ \AA}^3$. Attractive interactions correspond to negative values of ΔE_{ads} , which means a thermodynamically favored CO₂/H₂O binding to the MOF.

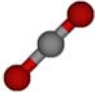
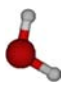
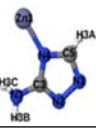
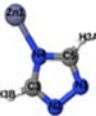
The interaction energy between the atoms was computed through the Lennard-Jones (LJ) potentials. This LJ potential is a simple pair potential, representing the London dispersion forces that can accurately model weak van der Waals bonds and has the following form:

$$V_{ij} = 4\epsilon_{ij} \left[\left(\frac{\sigma_{ij}}{r_{ij}} \right)^6 - \left(\frac{\sigma_{ij}}{r_{ij}} \right)^{12} \right],$$

where r_{ij} is the distance between interacting atoms i and j ; ϵ_{ij} and σ_{ij} are LJ potential parameters, i.e., the well depth and diameter at which the intermolecular potential between the two particles is zero, respectively. In the present contribution, the standard combining rules of Lorentz–Berthelot were considered to estimate the cross terms of the LJ parameters. LJ parameters for all atoms of MAF-66 and of ZTF were taken from the DREIDING²⁹ force field supplemented with zinc parameters from the Universal Force Field (UFF).³⁰ These parameters are listed in Table I together with the partial charges, which are obtained using DFT calculations and validated with available experimental values for MAF-66. Moreover, CO₂ was modeled as a rigid linear and three-center charged Lennard-Jones molecule. Partial charges and LJ parameters for CO₂ were taken from the TraPPE³¹ force field and are listed in Table I as well. For the studies of the water adsorption in ZTF, the TIP3P³² model was selected for H₂O molecules.

Monte Carlo simulations were used to compute the single adsorption isotherms of CO₂ and H₂O in MAF-66 and ZTF. Besides, we have also examined the adsorption of CO₂ in the presence of H₂O molecules. All simulations were performed with the Monte Carlo³³ suite of the RASPA code.³⁴ A cutoff distance of 12 Å was used for Lennard-Jones interactions. The Ewald sum technique was used to complete the electrostatic interactions. All simulations were performed by using 3 × 3 × 3 supercells and include random insertion, abstraction, and translation motions of molecules with equal probabilities. The simulations used 3 × 10⁵ equilibration and 6 × 10⁵ production cycles. GCMC simulations were carried on the PARADOX-IV supercomputing facility.³⁵ After inspection of the

TABLE I. Lennard-Jones parameters (ϵ/k_b in K and σ in Å) and partial atomic charges (q in e) of CO₂, of H₂O, and of [Zn–Atz] and [Zn–Tz], which are subunits of MAF-66 and ZTF. We give also the numbering used for the atoms.

CO ₂		Atom	O	C	H ₂ O		Atom	O	H			
		ϵ/k_b	79.0	27.0			ϵ/k_b	76.542	7.649			
		σ	3.05	2.80			σ	3.15	2.846			
		q	−0.35	0.70			q	−0.834	0.417			
[Zn–atz]		Atom	Zn1	N1	N2	N3	N4	C3	C5	H3A	H3B	H3C
		ϵ/k_b	62.399	38.149	38.149	38.149	38.149	47.856	47.856	7.649	7.649	7.649
		σ	2.4615	3.2626	3.2625	3.2626	3.2626	3.473	3.473	2.846	2.846	2.846
		q	1.108	−0.33	−0.33	−0.35	−0.35	0.0059	0.0059	0.08	0.08	0.08
[Zn–Tz]		Atom	Zn1	N1	N2	C3	N4	C5	H3A	H3B		
		ϵ/k_b	62.399	38.149	38.149	47.856	38.149	47.856	7.649	7.649		
		σ	2.4615	3.2626	3.2626	3.4730	3.2626	3.2626	2.846	2.846		
		q	1.118	−0.396	−0.396	0.0059	−0.398	0.0059	0.03	0.03		

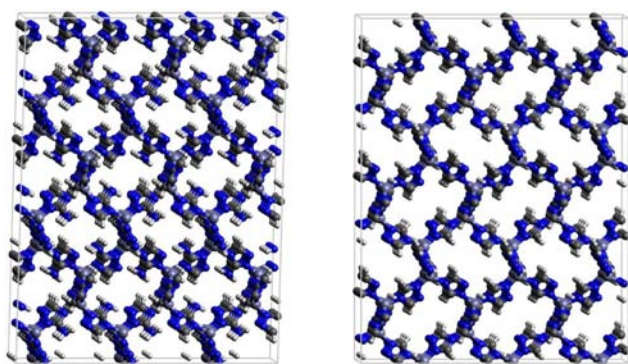


FIG. 1. DFT optimized 3D structures of MAF-66 (left) and of ZTF (right).

snapshots from the outputs of the GCMC simulations using the Avogadro program, we identified the interactions between the host and guest entities.

III. RESULTS AND DISCUSSIONS

A. Structural parameters of MAF-66 and ZTF

The GCMC simulations have been performed by using the DFT optimized structures of MAF-66 and ZTF, which are presented in Fig. 1. The 3D optimized structure of MAF-66 shows less than 1% change in the unit cell volume and 2% change in unit cell angles after optimization. We give in Table II the structural parameters of optimized MOFs (MAF-66 and ZTF), as well as the experimental geometrical parameters for the MAF-66 crystal structure given by Lin *et al.*⁵ Small differences of the main geometrical parameters are found between computed parameters of MAF-66 and those derived by the x-ray determinations of Lin *et al.* The calculated volumes inside the MOFs available for adsorption are 1329 Å³ for MAF-66 and 1383 Å³ for ZTF. For MAF-66 and ZTF, the pore sizes are computed as 0.41 nm and 0.46 nm, respectively (Fig. S2). The pore size value of the proposed MOF is within the 0.45 nm–2.0 nm window established by Yang *et al.*³⁶ for MOFs suitable for high CO₂ storage.

Besides, the helium void fraction and the surface area were computed with RASPA and also presented in Table II. Calculated void fractions for MAF-66 and ZTF were 0.457 and 0.507, respectively. These results show that the calculated void fraction for MAF-66 is in a satisfactory agreement with the experimentally measured void fraction (0.498). After optimization, we have, indeed, 0.041 (i.e., less than 10%) change in the void fraction. The surface areas are calculated as 1197 m²/g and 1800 m²/g for MAF-66 and ZTF, respectively. Although the two MOFs exhibit similar size pores and cavities, ZTF presents a distinctly larger surface area than MAF-66, which may favor higher gas uptake capacities.

B. Single molecule adsorption

1. Adsorption of CO₂ inside MAF-66 and ZTF under dry conditions

Figure 2 presents the adsorption positions of CO₂ molecules inside the pores of MAF-66 (left) and ZTF (right) after GCMC, together with nonbonded interactions between adsorbed host molecules and pores. CO₂ is adsorbed to the surface of the MAF-66 pore by two types of hydrogen bonds, either between oxygen of CO₂ with the closest hydrogen of the triazole 5-membered ring or between oxygen of CO₂ with the hydrogen of the amino group. These interactions depend on the orientation of CO₂ inside the pore. These findings are in line with the presence of two splitting peaks of the CO₂ band with red and blue shifts in the IR spectra of CO₂@MAF-66 recorded by Lin *et al.*⁵ Indeed, they documented the presence of two types of interactions of CO₂ within the MAF-66 pore: one as an electron acceptor through its carbon and another as an electron donor through its oxygen. Moreover, simulations indicate the presence of π stacking interaction between CO₂ and the aromatic ring of triazole, which can significantly enhance the adsorption of CO₂ in MOFs containing triazole (Fig. 2). Such nonbonded guest–host interactions are also found in ZTF (Fig. 2). Through the study of CO₂@Tz and CO₂@[Zn²⁺-Tz] gas phase clusters, we have found similar interactions and we have calculated the binding energies for C–H–O interactions that amount to about –8 kcal/mol.^{23,37} Moreover, the electrostatic interactions between the carbon of CO₂ and the nitrogen of the triazole ring (dipole–quadrupole interactions) with a distance of dC...N = 2.9 Å have also been found. π stacking interactions are more prominent in the CO₂-ZTF system than in the CO₂-MAF-66 system. This may

TABLE II. The unit cell parameters, unit cell volumes, and binding energies (per molecule) for adsorption of CO₂ inside MAF-66 and ZTF as calculated with SIESTA. We also give the helium void fractions and surface areas calculated with RASPA.

MOF	Method	a (Å)	b (Å)	c (Å)	α (°)	β (°)	γ (°)	Vol. (Å ³)	ΔE_{ads} (kcal/mol)	Helium void fraction	Surface area (m ² /g)
MAF-66	Calc. ^a	9.939	10.076	13.287	91.6	88.5	88.8	1329	–2.19	0.457	1197
	Exp. ^b	10.204	10.204	13.100	90.0	90.0	90.0	1364		0.498	1196
ZTF	Calc. ^a	10.25	10.22	13.20	90.7	89.9	89.6	1383	–1.96	0.507	1800

^aThis work.

^bReference 5.

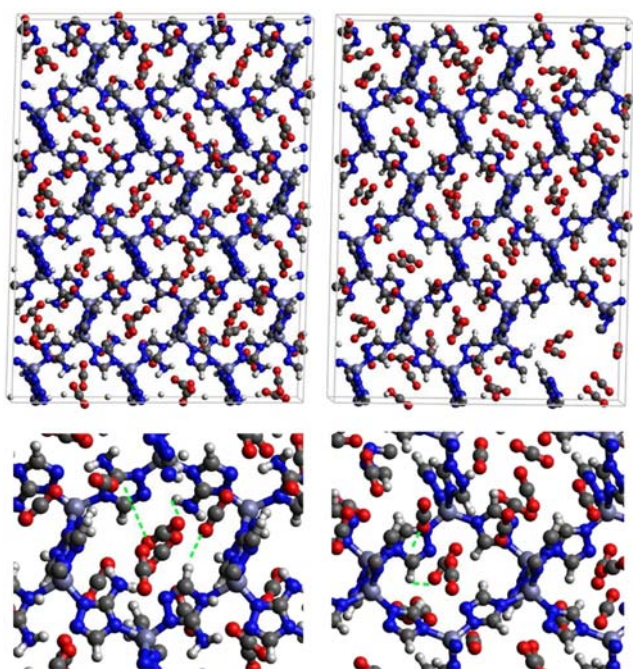


FIG. 2. (Top) GCMC adsorption sites of CO₂ molecules inside the pores of MAF-66 (left) and ZTF (right). (Bottom) Enlargement in the vicinity of CO₂ molecules where nonbonded interactions are also shown.

be the origin of the higher performance of ZTF for CO₂ uptake (see below).

GCMC simulations of CO₂ uptake at 253 K, 273 K, and 298 K temperatures were performed for experimentally reported and the DFT optimized MAF-66 structure and ZTF MOF. The shape of the adsorption isotherms can provide important details on the strength and type of interactions between the adsorbate molecule (CO₂) and the adsorbent surface (MOF cavity). Figure 3 displays the experimental and simulated adsorption isotherms of CO₂ inside MAF-66 at T = 273 K and T = 298 K and presents also comparison of the simulated adsorption isotherms of CO₂ in MAF-66 and in ZTF MOF at T = 253 K and T = 273 K.

As can be seen from Fig. 3, the simulated isotherms match nicely the experimental data at both 273 K and 298 K temperatures used for the experiments. This validates hence the force fields used for the simulations and proves that these force field parameters are accurate enough. The type of isotherms is concave with respect to the pressure axis and approaches a limiting adsorption saturation controlled by the accessible pore volume, pointing to the Langmuir adsorption isotherm model. This type of isotherms reflects a good adsorbate-adsorbent interaction. In addition, Fig. 3 shows that the adsorption of CO₂ decreases upon increasing the temperature in both MOFs.

The experimental amount⁵ of CO₂ adsorbed in MAF-66 at 1 atm and 273 K is measured 140 cm³ (STP) g⁻¹, which is a high adsorption capacity compared to that of other MOFs. Under the same conditions (T = 273 K, P = 1 atm), the CO₂ uptake of

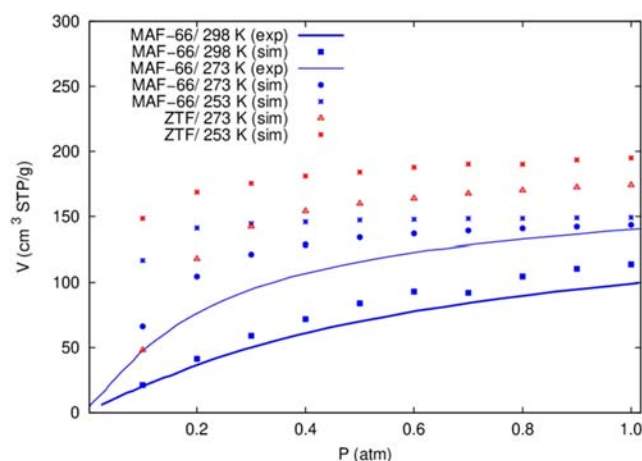


FIG. 3. Simulated (sim) and experimental (exp) adsorption isotherms of CO₂ in MAF-66 at 253 K, 273 K and 298 K, together with simulated isotherms of CO₂ in ZTF at 253 K and 273 K.

MAF-4, where the organic ligand is imidazole, is determined as 29.3 cm³ g⁻¹. For MAF-7, where the organic ligand is triazole, this amounts to 62.5 cm³ g⁻¹.¹³⁸ Both values are smaller to that of MAF-66. This is in line with the high capacities of MOFs with nitrogen rich organic ligands for CO₂ adsorption.

The simulated CO₂ uptake of MAF-66 at 1 atm and 273 K is equal to ~142 cm³ (STP) g⁻¹, which is close to the experimental data reported by Lin *et al.*,⁵ while for ZTF, the average absolute adsorption value of CO₂ is equal to ~174 cm³ (STP) g⁻¹ under the same conditions, i.e., more than 20% increase. Accordingly, the newly proposed MOF (ZTF) possesses higher CO₂ uptake capacities than MAF-66, MAF-4, and MAF-7 at higher pressure (P = 1 atm) and at 273 K under dry conditions. The better sequestration of CO₂ inside ZTF can be explained by the higher surface area (1800 m²/g) and volumetric capacity of ZTF (1383 Å³) in comparison with MAF-66 (1172 m²/g and 1329 Å³) due to making adsorption sites more accessible to CO₂ through the replacement of the amino group of the triazole ring by an hydrogen. Recently, Li *et al.*³⁹ synthesized a promising MOF with a nitrogen-rich octacarboxylate ligand, showing similar high affinity toward CO₂ (160.8 cm³ g⁻¹ at 273 K and 1 atm.), which has been verified by gas adsorption and Raman spectral detections. Under the same conditions, other promising MOFs with the formula of [Cu₂(L)]_n, consisting of four-connected unsaturated paddle-wheel Cu₂ clusters and four-connected nitrogen-rich L ligands, namely, for NTU-111, NTU-112, and NTU-113, were reported by the same group,⁴⁰ showing interestingly high affinities toward CO₂ adsorption of 124.6 cm³ g⁻¹, 158.5 m³ g⁻¹, and 166.8 cm³ g⁻¹, respectively.

In addition to GCMC data, we have calculated binding energies of one CO₂ molecule in MAF-66 and ZTF (Table II) by using the procedure described in Sec. II.⁴¹ As shown in Table II, calculated adsorption energies for MAF-66 and ZTF are -2.19 kcal/mol and -1.96 kcal/mol, respectively. Accordingly, both MAF-66 and ZTF structures favor the adsorption of carbon dioxide molecules, mainly due to the interactions between the CO₂ and the functional groups.

Optimized structures of ZTF and MAF-66 with one CO₂ molecule inside cavity are presented in Fig. S3. Figure S3 shows that CO₂ molecules prefer to link the hydrogen atoms of ZTF and MAF-66, which is in line with the GCMC results (Fig. 2).

2. Adsorption of H₂O inside MAF-66 and ZTF

Figure 4 presents the adsorption positions of H₂O molecules inside the pores of MAF-66 (left) and ZTF (right) after GCMC simulations, together with the nonbonded interactions between adsorbed hosted molecules and pores. The H₂O molecules are stabilized in the pores of MAF-66 by two types of hydrogen bonds: either between the oxygen of H₂O and the hydrogen of the amino group of Tz or between the nitrogen of the MOF subunit and the hydrogen of H₂O. In the case of ZTF, we identified the presence of hydrogen bonds between the hydrogen of H₂O and the nitrogen of Tz and between the oxygen of H₂O and the hydrogen of C-(Tz) (Fig. 4). Through the study of the H₂O@[Zn²⁺-Tz] clusters, we also recently characterized such types of interactions within these complexes. We also showed that the N as a preferential adsorption site may be related to the larger values of the binding energies for the N-H-O interactions (>10 kcal/mol) compared to the C-H-O water Tz H bond.²³

GCMC simulations were performed to calculate the H₂O adsorption isotherms in MAF-66 and ZTF at 273 K. Simulated adsorption isotherms are presented in Fig. 5. This figure shows that there are two regimes: (i) for P < 0.6 atm, ZTF has distinctly lower H₂O uptake in comparison with MAF-66; (ii) for P > 0.6 atm, both MOFs exhibit similar H₂O uptake while ZTF shows a slightly higher

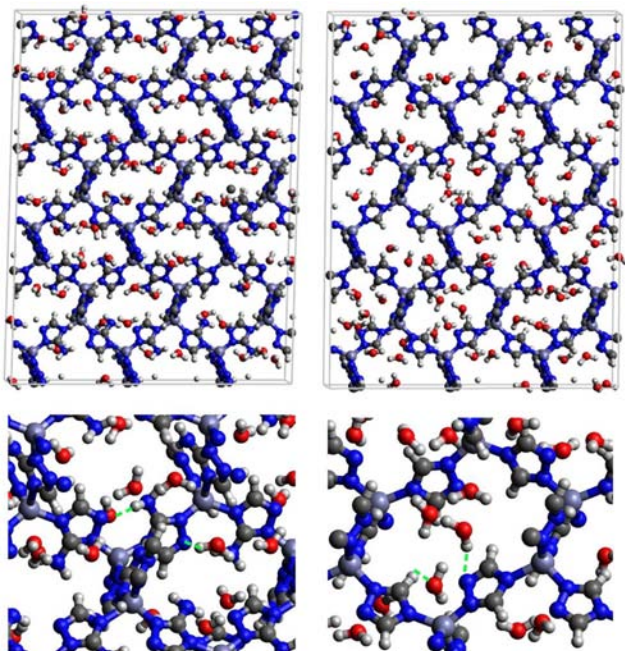


FIG. 4. (Top) GCMC adsorption sites of H₂O molecules inside the pores of MAF-66 (left) and ZTF (right). (Bottom) Enlargement in the vicinity of H₂O with nonbonded interactions are also presented.

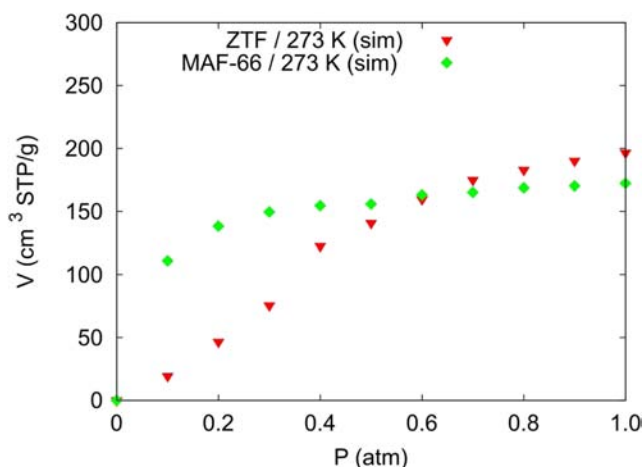


FIG. 5. Simulated adsorption isotherms of H₂O in MAF-66 and ZTF at 273 K.

capacity. Nevertheless, the differences between both MOFs remain small.

Water adsorption loadings at low pressure can be used to determine relative hydrophobicity among adsorbents. As shown in Fig. 5, the greater sharpness of the isotherm of MAF-66 is due to the higher affinity of the MAF-66 adsorbent than that of the ZTF adsorbent, which hence adsorbs more H₂O molecules in comparison to ZTF (at least at low pressure). These findings may be explained by the presence of the hydrophilic NH₂ group in MAF-66 subunits that attracts H₂O molecules at lower pressures, whereas at higher water upload, a competition occurs, within the pores, where H₂O molecules either interact mutually or adsorb to the surface. In the former case, water clusters are formed that transit through the cavities and do not attach to the MOF surface cavity. Such effects of functional groups on water adsorption behavior were already noticed by Liu *et al.*⁴²

C. Co-adsorption of CO₂/H₂O inside ZTF

The effect of water on the adsorption of carbon dioxide inside ZTF is investigated in two different ways. First, we performed simulations, where the H₂O molecules were introduced at the active sites in ZTF such as the coordinatively unsaturated Zn atoms and the uncoordinated N atom of the triazolate ring. Second, we considered the adsorption of CO₂ with preloaded N_{water} H₂O molecules (CO₂-H₂O mixture). While the number of CO₂ molecules varies in the course of the simulation, the number of H₂O molecules is not. H₂O molecules were also allowed to move within the cavities of these MOFs until reaching equilibrium.

Initial structures of ZTF with the addition of H₂O molecules used for GCMC simulations were optimized by using DFT calculations and are presented in Fig. 6. Table III gives the optimized unit cell parameters of MOFs with H₂O molecules inside the unit cells. This table shows that both optimized structures are close with the slightly higher volume cell in the case of the structure with H₂O molecules around Zn.

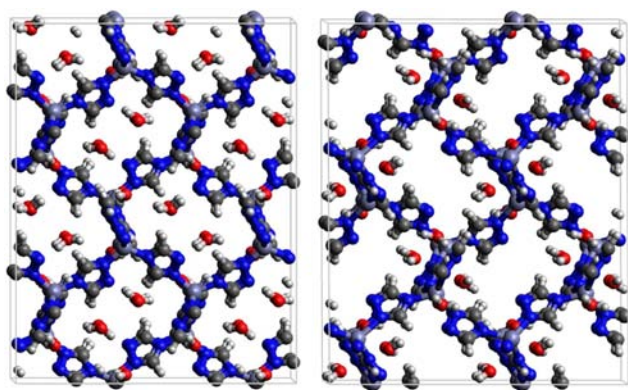


FIG. 6. DFT optimized structures of ZTF with H₂O pre-located near the nitrogen of the Tz subunit (left) and with H₂O in the vicinity of the zinc atom (right).

1. CO₂ adsorption in ZTF with active sites occupied by H₂O molecules

We performed GCMC simulations to evaluate the CO₂ adsorption isotherms for the hydrated ZTF MOF at 273 K. Here, we report the GCMC results of the influence of the H₂O molecules on CO₂ adsorption that occupy either the coordinatively unsaturated Zn atoms or the uncoordinated N atom of the triazolite ring active sites. The corresponding simulated adsorption isotherms of CO₂ at 273 K in ZTF with and without the presence of H₂O molecules in two different positions are presented in Fig. 7. This figure shows that the CO₂ uptake significantly decreases when H₂O molecules are located in the vicinity of nitrogen of the triazole subunit. Indeed, when going from dry to hydrated conditions at higher pressures ($P \sim 1$ atm), the average absolute adsorption values of CO₂ significantly decreased from ~ 174 cm³ (STP) g⁻¹ to ~ 73 cm³ (STP) g⁻¹ when H₂O interacts with nitrogen through the N–H(OH) hydrogen bond. This indicates the crucial role of this nitrogen as a potential site for CO₂ sequestration within the ZTF cavity. Thus, our results suggest that this nitrogen is among the preferential sites within the pore for CO₂ adsorption.

When H₂O molecules are coordinated with the Zn atom, the situation is quite different, where we have close to constant evolution of V over the 0.1 atm–1 atm pressure domain. Compared to a dry ZTF, we may identify three regimes:

- (i) “Very low pressure” for $P < 0.15$ atm: in both cases, the presence of water increases the adsorption of CO₂ in ZTF (Fig. 7). This observation has been confirmed also by Liu *et al.*⁴² and was explained by the contribution of electrostatic interactions especially at these low pressures. These interactions arise from the quadrupole moment of CO₂ interacting with the electric field gradient of the sorbent, which is enhanced especially when H₂O occupies the Zn open-metal site. This is in line also with the findings of Yazaydin *et al.*²⁵
- (ii) “Low pressure” for $0.15 < P < 0.5$ atm: the dry ZTF presents lower capacities for the CO₂ uptake than the hydrated case. For instance, the CO₂ uptake increases from 118.1 cm³ (STP) g⁻¹ at $P = 0.2$ atm and $T = 273$ K in dry conditions to 158.4 cm³ (STP) g⁻¹ in the presence of water. Thus, the presence of H₂O molecules attached to the Zn sites enhances the CO₂ adsorption. Local water induced modifications of the CO₂–surface pore potential interactions are in favor of attaching the CO₂ molecules.
- (iii) “High pressure” for $P > 0.5$ atm: the presence of water seems not to have any influence on the CO₂ uptake. A plateau is observed around 170 cm³ (STP) g⁻¹. This is the signature of a saturation of the CO₂ adsorption of the available sites.

To explain this result, we present in Fig. 8 the DFT based GCMC adsorption sites of CO₂ molecules inside the pores of ZTF in the presence of H₂O molecules near the zinc or nitrogen atoms of the [Zn–Tz] subunits. A close examination of this figure reveals the occurrence of several types of interactions that contribute to the CO₂ capture. First, one may see several hydrogen bonds. Let us cite, for instance, the hydrogen bonds between the oxygen of CO₂ and the hydrogen of H₂O with $d\{\text{O}_{\text{CO}_2}\text{--H}_{\text{H}_2\text{O}}\}$ distances in the [2.7–3.2] Å range. We also characterized hydrogen bonds between the oxygen of CO₂ and the hydrogen of Tz, C–H–O(CO₂), with $d\{\text{O}_{\text{CO}_2}\text{--H}_{\text{C}}\}$ distances in the [2.6–3.5] Å range. Second, Fig. 8 shows the presence of π stacking interactions between the CO₂ molecule and the aromatic ring of the Tz subunits. Third, there are electrostatic interactions between the carbon of CO₂ and the unprotonated nitrogen of Tz with $d\{\text{O}_{\text{CO}_2}\text{--N}_{\text{Tz}}\}$ in the $\sim [2.85\text{--}3.4]$ Å range.

When H₂O is placed near the nitrogen of Tz, the hydrogen bonding is favored between the hydrogen of H₂O and the unprotonated nitrogen of Tz with intermolecular distances of $\sim [1.78\text{--}1.81]$ Å. The significant decrease in CO₂ capture in this case (Fig. 8) indicates that the sites around the nitrogen

TABLE III. Computed unit cell parameters and volume (V) of ZTF with and without the presence of water molecules. Distances and binding energies (per molecule) between water and ZTF are also given.

ZTF	a (Å)	b (Å)	c (Å)	α (°)	β (°)	γ (°)	V (Å ³)	$d_{(\text{N-H})}$ (Å)	$d_{(\text{Zn-O})}$ (Å)	ΔE_{ads} (kcal/mol)
Without H ₂ O	10.25	10.22	13.20	90.68	89.93	89.6	1383			
With H ₂ O ^a	10.15	9.73	12.97	90.72	90.10	89.94	1281	1.8	1.8	-12.12^b
With H ₂ O ^c	10.17	10.60	12.79	89.76	90.37	86.90	1377	2.2	3.8	-12.19

^aGeometrical parameters of the ZTF unit cell when H₂O is located near nitrogen.

^bCalculated binding energy of one water and MAF-66 is -13.03 kcal/mol.

^cGeometrical parameters of the ZTF unit cell when H₂O interacts with zinc.

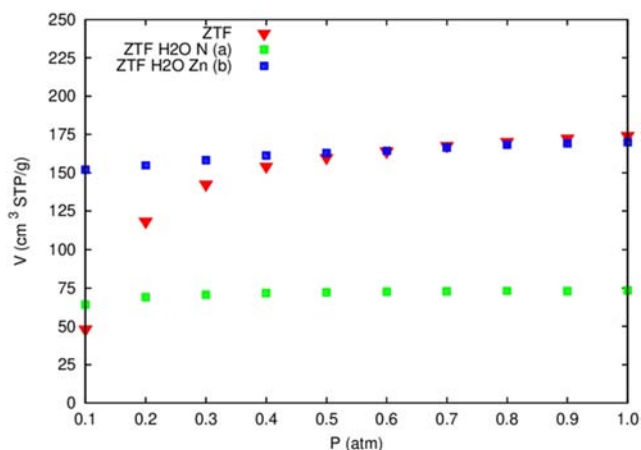


FIG. 7. Simulated adsorption isotherms of CO₂ at 273 K in ZTF with and without the presence of H₂O molecules in two different positions. In (a), H₂O is located near nitrogen, and in (b), H₂O is located in the vicinity of the Zn atom.

atom contribute to the adsorption of CO₂ through nonbonded interactions between the carbon of CO₂ and the unprotonated nitrogen of Tz. This does not prevent the presence of weak interactions between CO₂ and ZTF like π stacking interactions

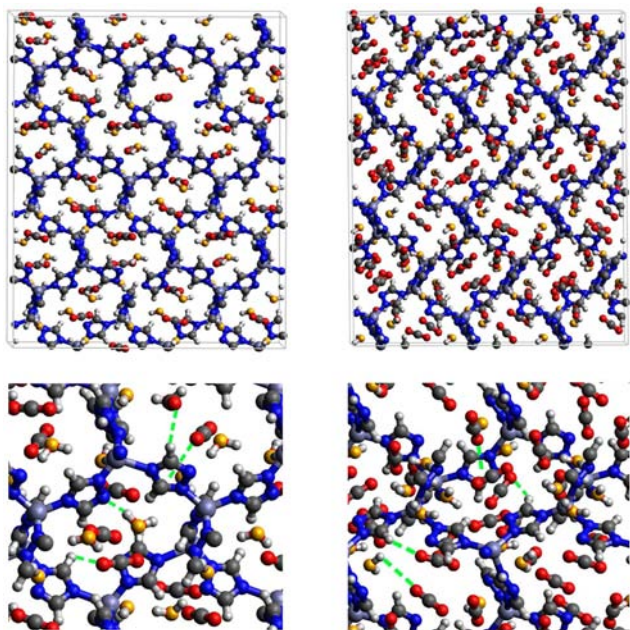


FIG. 8. (Top) GCMC adsorption sites of CO₂ molecules inside the pores of ZTF in the presence of H₂O near the nitrogen atom of the triazole subunits (left). GCMC adsorption sites of CO₂ molecules inside the pores of ZTF in the presence of H₂O near the Zn site (right). (Bottom) Enlargement in the vicinity of CO₂ and H₂O where nonbonded interactions are also highlighted. For better clarity, we artificially colored the O atoms of CO₂ in red and that of H₂O in yellow.

between CO₂ and the aromatic rings of Tz and hydrogen bonding between the hydrogen of Tz and the oxygen of CO₂, C–H–O(CO₂) with $d \sim [2.5\text{--}3.2]$ Å. Recently, some of us showed that this kind of interactions occurs within the CO₂@[Zn²⁺–Tz] gas phase clusters.³⁷ We also showed through the investigations of the CO₂@H₂O@[Zn²⁺–Tz] clusters that water induces changes in the binding energies of these complexes when H₂O is attached to the Zn cation. The influence of water takes place through weak interactions as those found here for the 3D ZTF porous material.²³

According to Table III, DFT calculated E_{ads} of one water molecule inside ZTF for two investigated positions are similar (around –12 kcal/mol). Our computations reveal that the adsorption of one water molecule per unit cell is favorable in studied ZTF and MAF-66 (Table III) for both investigated initial positions of water. Figure S4 shows the DFT optimized structure of one water molecule in MAF-66.

2. CO₂ adsorption with a fixed number of preloaded water molecules inside the ZTF pore

We performed several simulations where we varied the number of the preloaded H₂O molecules (N_{water}) inside the ZTF cavity. Table IV gives the results of the CO₂ adsorption in the ZTF model MOF by varying N_{water} from 0 to 100. All simulations were performed at a temperature of 273 K and for very low (0.1 atm) and high pressures (1 atm). Table IV shows that at very low pressure, increasing the number of H₂O molecules up to 20 slightly increases the amount of adsorbed CO₂ [from ~48 cm³ (STP) g^{–1} to ~52 cm³ (STP) g^{–1}]. Beyond this preloaded amount of H₂O, the CO₂ uptake starts to decrease. This behavior was also observed by Zhang *et al.*³⁸ For explanation, these authors proposed that the interaction between the quadrupole moment of CO₂ and the electric field created by H₂O molecules increases the CO₂ uptake. At higher pressure ($P = 1$ atm), water and carbon dioxide compete in adsorption sites. Calculations show that increasing the number of H₂O molecules acts to decrease the adsorption of CO₂ in ZTF from ~174 cm³ (STP) g^{–1} (without H₂O molecules) to ~123 cm³ (STP) g^{–1} (with 100 H₂O molecules). The reduction of CO₂ adsorption at higher pressures in the presence of adsorbed water can be attributed to the stronger binding interactions for H₂O@[Zn²⁺–Tz] complexes compared to the CO₂@[Zn²⁺–Tz] ones. For instance, some of us showed recently that the binding energies of gas phase H₂O@[Zn²⁺–Tz] complexes are larger by >20 kcal/mol than those computed for

TABLE IV. Average adsorption amount of CO₂ [in cm³ (STP) g^{–1}] in ZTF at $T = 273$ K with and without the presence of H₂O molecules for pressures (P) of 0.1 atm and 1 atm. N_{water} is the number of preloaded H₂O molecules inside the pore.

N_{water}	0	10	20	50	100
H ₂ O ^a	0	7.778	15.557	38.892	77.784
$P = 0.1$ atm	48.038	50.783	51.698	48.156	41.456
$P = 1$ atm	174.155	169.519	164.092	148.893	123.363

^aThe average adsorption amount of H₂O [in cm³ (STP) g^{–1}].

$\text{CO}_2@[\text{Zn}^{2+}-\text{Tz}]$.²³ Moreover, the simulations can provide a molecular explanation for this reduced uptake of CO_2 in the presence of adsorbed water. At higher pressure, when water adsorbs to triazole sites, it is held relatively fixed with one of the hydrogen atoms directed toward the nitrogen atom of Tz or with oxygen atom directed toward the hydrogen atom of Tz, as shown in Fig. 8, and CO_2 is unable to adsorb into the same adsorption positions of the cell as H_2O .

IV. CONCLUSIONS

In this work, we used *in silico* methodology to design a new MOF by modifying the well-known MAF-66 targeting better CO_2 adsorption capacities with and without the presence of water. We thus studied the carbon dioxide and water adsorption in both zinc triazolate based frameworks, considering the two adsorbent species simultaneously or alternatively. We have shown here, by using GCMC simulations, that the newly designed ZTF MOF composed of triazolate as the organic ligand and Zn(II) as the metal linker has higher CO_2 adsorption capacity at high pressure under dry conditions, at 273 K. This sequestration is associated with several types of interactions such as electron acceptor–electron donor interaction between the carbon of CO_2 and the nitrogen of Tz of ZTF and π stacking interactions between CO_2 and aromatic rings of Tz and hydrogen bonds as found for ZIFs.⁴¹ GCMC simulations of adsorption of water in both MAF-66 and ZTF structures show that water possesses more favorable adsorption ability than carbon dioxide, which is confirmed by the DFT calculated binding energy of one water molecule with investigated MOFs when compared to the adsorption of one CO_2 molecule. Besides, the significant decrease in CO_2 capture when the H_2O molecule is near the nitrogen of Tz in ZTF shows that the sites around nitrogen contribute to the adsorption of CO_2 through nonbonded interactions between carbon of CO_2 and unprotonated nitrogen of Tz.

Moreover, pre-adsorbing small amount of H_2O molecules at low pressure increases the capacity of the MOF for CO_2 uptake, associated with the electrostatic interaction between the quadrupole moment of CO_2 and the electric field created by H_2O molecules. At higher pressure and hydrated conditions, the CO_2 uptake slightly decreases while increasing the number of H_2O molecules. Calculations show that the H_2O molecule affinity inside these structures is so strong that it can displace the adsorbed CO_2 molecules. In general, it seems that water and carbon dioxide compete in some adsorption sites, but mainly, the high adsorption of CO_2 and H_2O inside the investigated triazoles is due to its very high surface area and the established hydrogen bonds between the hosted molecules and the MOF surfaces.

SUPPLEMENTARY MATERIAL

This section contains the four following figures: Figure S1: Convergence of the total energy with the plane wave cutoff and k point sampling mesh for MAF-66. Figure S2: Pore size distributions of MAF-66 (left) and ZTF (right). Figure S3: DFT optimized structures of parts of the supercells of ZTF (left) and MAF-66 (right) with one

CO_2 molecule inside. Figure S4: DFT optimized structure of parts of the supercell of MOF-66 with one water molecule inside.

DEDICATION

This paper is dedicated to the memory of Professor Salima Boughdiri who passed away on April 4, 2020.

ACKNOWLEDGMENTS

S.G. and I.D. acknowledge support of the Serbian Ministry of Education and Science (Grant No. 451-03-68/2020-14/200026). We thank the COST Action CA17120 Chemobionics (CBrio) of the European Community for support. This work was supported by a STSM Grant from COST Action CA17120.

DATA AVAILABILITY

The data that support the findings of this study are available within the article and its [supplementary material](#).

REFERENCES

- 1 R. Quadrelli and S. Peterson, *Energy Policy* **35**, 5938–5952 (2007).
- 2 S. Choi, J. H. Drese, and C. W. Jones, *ChemSusChem* **2**, 796–854 (2009).
- 3 Y. Liu, Z. U. Wang, and H.-C. Zhou, *Greenhouse Gases: Sci. Technol.* **2**, 239–259 (2012).
- 4 B. Chen, S. Xiang, and G. Qian, *Acc. Chem. Res.* **43**, 1115–1124 (2010).
- 5 R.-B. Lin, D. Chen, Y.-Y. Lin, J.-P. Zhang, and X.-M. Chen, *Inorg. Chem.* **51**, 9950–9955 (2012).
- 6 E. Stavitski, E. A. Pidko, S. Couck, T. Remy, E. J. M. Hensen, B. M. Weckhuysen, J. Denayer, J. Gascon, and F. Kapteijn, *Langmuir* **27**, 3970–3976 (2011).
- 7 P. Serra-Crespo, E. V. Ramos-Fernandez, J. Gascon, and F. Kapteijn, *Chem. Mater.* **23**, 2565–2572 (2011).
- 8 J. Jiang and O. M. Yaghi, *Chem. Rev.* **115**, 6966–6997 (2015).
- 9 L. Joos, J. A. Swisher, and B. Smit, *Langmuir* **29**, 15936–15942 (2013).
- 10 G. Li, P. Xiao, P. A. Webley, J. Zhang, and R. Singh, *Energy Procedia* **1**, 1123–1130 (2009).
- 11 G. Li, P. Xiao, P. Webley, J. Zhang, R. Singh, and M. Marshall, *Adsorption* **14**, 415–422 (2008).
- 12 E. Gonzales - Zamora and I. A. Ibarra, *Mater. Chem. Front.* **1**, 1471–1484 (2017).
- 13 E. Soubeyrand-Lenoir, C. Vagner, J. W. Yoon, P. Bazin, F. Ragon, Y. K. Hwang, C. Serre, J.-S. Chang, and P. L. Llewellyn, *J. Am. Chem. Soc.* **134**, 10174–10181 (2012).
- 14 N. C. Burtch, H. Jasuja, and K. S. Walton, *Chem. Rev.* **114**, 10575–10612 (2014).
- 15 R. Vaidhyanathan, S. S. Iremonger, K. W. Dawson, and G. K. H. Shimizu, *Chem. Commun.* **35**, 5230–5232 (2009).
- 16 A. Demessence, D. M. D'Alessandro, M. L. Foo, and J. R. Long, *J. Am. Chem. Soc.* **131**, 8784–8786 (2009).
- 17 M. A. Hussain, Y. Soujanya, and G. N. Sastry, *J. Phys. Chem. C* **119**, 23607–23618 (2015).
- 18 K. D. Vogiatzis, A. Mavrandonakis, W. Klopffer, and G. E. Froudakis, *Chem. Phys. Chem.* **10**, 374–383 (2009).
- 19 D. Liu, Y. Wu, Q. Xia, Z. Li, and H. Xi, *Adsorption* **19**, 25–37 (2013).
- 20 Y. Lin, C. Kong and L. Chen, *RSC Adv.* **6**, 32598–32614 (2016).
- 21 X.-J. Wang, P.-Z. Li, Y. Chen, Q. Zhang, H. Zhang, X. X. Chan, R. Ganguly, Y. Li, J. Jiang, and Y. Zhao, *Sci. Rep.* **3**, 1149 (2013).
- 22 J.-J. Liu, X. He, M. Shao, and M.-X. Li, *J. Mol. Struct.* **891**, 50–57 (2008).

- ²³R. Dahmani, S. Grubišić, S. B. Yaghlane, S. Boughdiri, and M. Hochlaf, *J. Phys. Chem. A* **123**, 5555–5565 (2019).
- ²⁴R. Dahmani, S. Ben Yaghlane, S. Boughdiri, M. Mogren Al-Mogren, M. Prakash, and M. Hochlaf, *Spectrochim. Acta, Part A* **193**, 375–384 (2018).
- ²⁵A. Ö. Yazaydın, A. I. Benin, S. A. Faheem, P. Jakubczak, J. J. Low, R. R. Willis, and R. Q. Snurr, *Chem. Mater.* **21**, 1425–1430 (2009).
- ²⁶E. Artacho, E. Anglada, O. Diéguez, J. D. Gale, A. García, J. Junquera, R. M. Martin, P. Ordejón, J. M. Pruneda, D. Sánchez-Portal, and J. M. Soler, *J. Phys.: Condens. Matter* **20**, 064208 (2008).
- ²⁷E. Artacho, D. Sánchez-Portal, P. Ordejón, A. García, and J. M. Soler, *Phys. Status Solidi B* **215**, 809–817 (1999).
- ²⁸J. P. Perdew, K. Burke, and M. Ernzerhof, *Phys. Rev. Lett.* **77**, 3865–3868 (1996).
- ²⁹S. L. Mayo, B. D. Olafson, and W. A. Goddard, *J. Phys. Chem.* **94**, 8897 (1990).
- ³⁰A. K. Rappe, C. J. Casewit, K. S. Colwell, W. A. Goddard, and W. M. Skiff, *J. Am. Chem. Soc.* **114**(25), 10024–10035 (1992).
- ³¹J. J. Potoff and J. I. Siepmann, *AIChE J.* **47**, 1676 (2001).
- ³²W. L. Jorgensen, J. Chandrasekhar, J. D. Madura, R. W. Impey, and M. L. Klein, *J. Chem. Phys.* **79**, 926 (1983).
- ³³D. Dubbeldam, A. Torres-Knoop, and K. S. Walton, *Mol. Simul.* **39**, 1253–1292 (2013).
- ³⁴D. Dubbeldam, S. Calero, D. E. Ellis, and R. Q. Snurr, *Mol. Simul.* **42**, 81–101 (2016).
- ³⁵PARADOX IV cluster at the Scientific Computing Laboratory of the Institute of Physics Belgrade, supported in part by the Serbian Ministry of Education and Science under project No. ON171017.
- ³⁶Q. Yang, C. Zhong, and J.-F. Chen, *J. Phys. Chem. C* **112**, 1562–1569 (2008).
- ³⁷R. Boulmène, M. Prakash, and M. Hochlaf, *Phys. Chem. Chem. Phys.* **18**, 29709–29720 (2016).
- ³⁸J.-P. Zhang, A.-X. Zhu, R.-B. Lin, X.-L. Qi, and X.-M. Chen, *Adv. Mater.* **23**, 1268–1271 (2011).
- ³⁹P.-Z. Li, X.-J. Wang, J. Liu, J. S. Lim, R. Zou, and Y. Zhao, *J. Am. Chem. Soc.* **138**, 2142–2145 (2016).
- ⁴⁰P.-Z. Li, X.-J. Wang, K. Zhang, A. Nalaparaju, R. Zou, R. Zou, J. Jiang, and Y. Zhao, *Chem. Commun.* **50**, 4683–4685 (2014).
- ⁴¹V. Timón, M. L. Senent, and M. Hochlaf, *Microporous Mesoporous Mater.* **218**, 33–34 (2015).
- ⁴²D. Liu, C. Zheng, Q. Yang, and C. Zhong, *J. Phys. Chem. C* **113**, 5004–5009 (2009).